Microstructural analysis of the radial distribution function for liquid and amorphous Al

2003 J. Phys.: Condens. Matter 15 2259

(http://iopscience.iop.org/0953-8984/15/14/302)

INSTITUTE OF PHYSICS PUBLISHING JOURNAL OF PHYSICS: CONDENSED MATTER

J. Phys.: Condens. Matter **15** (2003) 2259–2267 PII: S0953-8984(03)57458-6

Microstructural analysis of the radial distribution function for liquid and amorphous Al

G X Li, Y F Liang, Z G Zhu and C S Liu

Laboratory of Internal Friction and Defects in Solids, Institute of Solid State Physics, Chinese Academy of Sciences, PO Box 1129, Hefei 230031, People's Republic of China

Received 13 December 2002
Published 31 March 2003
Online at stacks.iop.org/JPhysCM/15/2259

Abstract

Constant-pressure molecular dynamics simulations and analysis of the local atomic structures have been performed to study the conventional and 'inherent' structural evolution of liquid Al during rapid solidification. The results show that the radial distribution functions $g(r)$ exhibit a second-peak splitting feature not only for the general structures of the amorphous states but also for the inherent structure of liquid states. The second peak of $g(r)$ decomposes into three main components, each corresponding to different pairs. The first subpeak in the inherent structure of the liquid arises from 2211 and 2331 pairs (which correspond to triangles with a common side and the tetrahedra sharing a face respectively), while the first subpeak in the amorphous state arises from 2331 pairs; in both cases the second subpeak is due to the 2101 pairs (linear trimers). The existence of a shoulder or the splitting in the second peak of $g(r)$ in the amorphous state, and even in the undercooled liquid state, results mainly from the increase in number of and aggregation of the tetrahedra, which in turn give rise to the presence of entities with local icosahedral order.

1. Introduction

It is well known experimentally that the structural properties of amorphous and liquid metals show similar general features, which are characterized by a shoulder in the second peak or the splitting of the second peak observed both in the structure factor, $S(Q)$, and in the radial distribution function, $g(r)$ [1]. The $S(Q)$ or $g(r)$ obtained from experimental data, such as x-ray scattering data, gives us limited information about the short-range order because of the complexity of the structure. So, despite numerous experimental and theoretical attempts to determine the structural nature of liquids and glasses, until now no satisfactory understanding has been attained about similarities and differences in the microstructures of amorphous and liquid metals from the atomistic point of view. For example, the nearest-neighbour coordination number (N), determined by integration over the whole area between the first and the second

minimum of $g(r)$, is about 12 for simple liquid and glass metals, but a value of 12 for N is characteristic of several types of densely packed short-range order, e.g., icosahedral, fcc, and hcp structures. Molecular dynamics simulations can generate realistic structural models for amorphous materials and provide detailed information about their atomic structures, which allows us to further analyse the microstructural details responsible for various features in the $g(r)$ [2–5].

In the present work, we present results of a microstructural study of liquid Al during rapid solidification using molecular dynamics simulations and conjugate gradient energy minimization to find the inherent structures. The main goal of this work is to investigate the structural changes when the splitting of the second peak in $g(r)$ occurs, in the hope of gaining an understanding of the splitting mechanism of the second peak in $g(r)$ on the atomic level. The rest of the paper is organized as follows. In section 2, we sketch out the main computational methods. In section 3 we present and discuss the results obtained. Finally, we give a brief summary in section 4.

2. Computational methods

The Al atomic interactions are modelled through the *glue* potential [6], which can correctly reproduce many basic properties of Al in crystalline and noncrystalline phases. Using this potential, Sun and Gong have successfully studied the structural properties and glass transition in Al clusters [7]; Liu *et al* [8] have investigated the cooling rate dependence of some microscopic and macroscopic quantities of liquid Al during rapid solidification. Constant-pressure molecular dynamics simulations were performed on a system consisting of 500 Al atoms in a cubic cell under periodic boundary conditions. The Newtonian equations of motion were integrated using the velocity Verlet algorithm with a time step $t = 5.3 \times 10^{-16}$ s. First the system was gradually heated up to 2289 K starting from the perfect crystal. Next the system was run for 50 000 time steps to guarantee an equilibrium liquid state. Then the system was cooled at a rate of 9.5×10^{12} K s^{-1}. At each sampling temperature, the system first experienced a relaxation process of 50 000 steps and another 12 000-time-step run was performed to collect data for 20 configurations for analysing microscopic quantities using another program.

The system microstructures were described by the pair analysis technique [9], using a set of four indices[1], which allows one to decompose the first and second peaks of the $g(r)$. Type I pairs (the first index is 1) are responsible for the first peak of $g(r)$ and type II pairs (the first index is 2) for the second peak. (The typical pairs of type I are 1551, 1541 and 1431, 1421, and 1422 pairs. The 1551 pair characterizes the icosahedron-like local structure. The 1421 and 1422 pairs respectively represent the fcc-like and hcp-like local structures. The 1541 and 1431 pairs represent the icosahedral defect and fcc defect local structures. For details see figure 1 in [8] and figure 3 in [9]. The main pairs of type II are 2101, 2211, and 2331 pairs.) The 2101 pair represents a linear trimer; the 2211 and 2331 pairs characterize two triangles with a common side and two tetrahedra sharing a face. In addition, to suppress the vibrational motion effect due to high temperatures when analysing the liquid structures, we use the concept of inherent structure introduced by Stillinger and Weber [10], which is defined as local minimum configurations of the potential energy surface and can be reached by conjugate gradient energy minimization. The idea of resolving observable order in liquid into the vibration and the inherent structural parts offers a useful way to classify their microstructures and to discover the kinds of short-range order in many materials [11, 12].

[1] The first integer denotes to what peak of $g(r)$ the pair under consideration belongs. The second integer is the number of common nearest neighbours of that pair. The third integer is the number of nearest-neighbour bonds found between the number of particles denoted by the second index. The fourth integer is used to distinguish the pair when the former three integers are not sufficient. The 1551 pair characterizes the icosahedron-like local structure; the 1421 and 1422 pairs represent the fcc-like and hcp-like local structures.

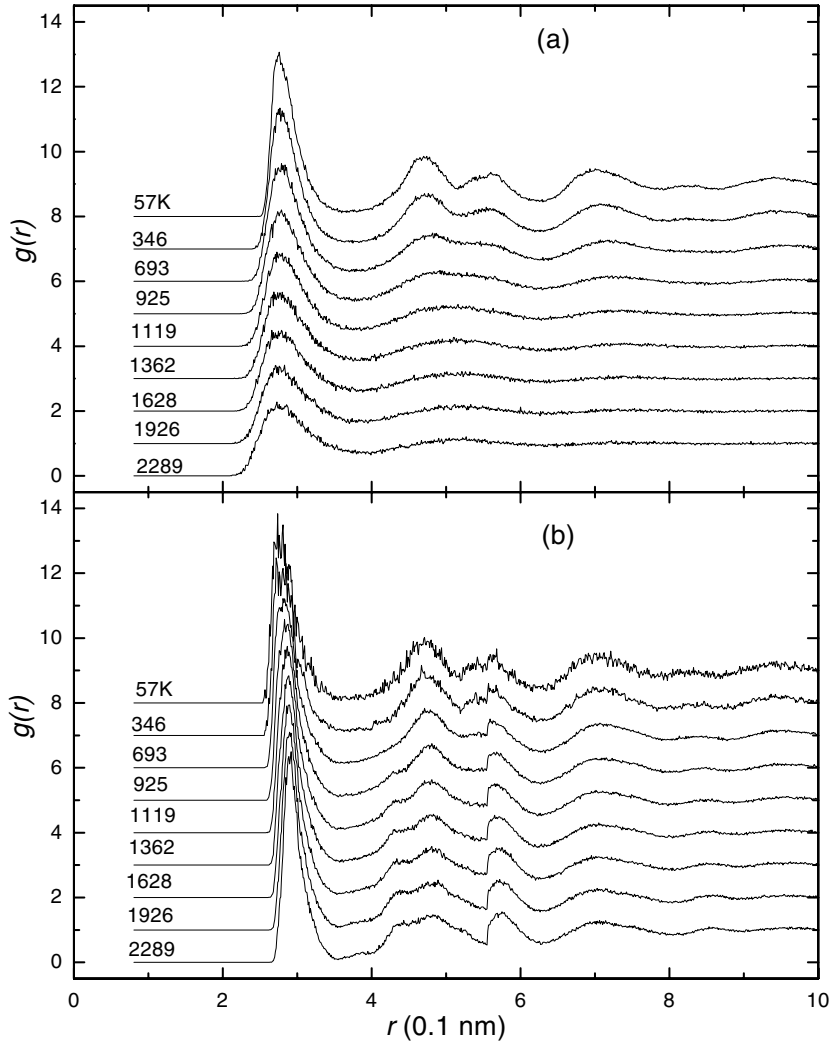

Figure 1. Examples of radial distribution functions $g(r)$ of liquid or amorphous Al (a) and their corresponding inherent structures (b).

3. Results and discussion

Typical examples of the $g(r)$ for liquid Al during rapid solidification and their corresponding $g(r)$ obtained by the inherent structure mechanism are presented in figures 1(a) and (b), respectively. Note that the glass transition temperature T_g is about 550 K, deduced from the temperature dependence of the enthalpy as in the [2]. From figure 1(a), the first peak of $g(r)$ perceptibly sharpens as the temperature decreases; a shoulder on the right-hand side of the second peak is observed in the $g(r)$ at 925 K; this shoulder becomes more pronounced with lowering temperature and then the splitting of the second peak takes place. From figure 1(b), in the corresponding inherent structures the $g(r)$ shows an enhanced first peak and a second-peak splitting feature not only for glass states but also for liquid states, the feature in the liquid state being insensitive to the temperature. Figure 2 shows the relative number of various

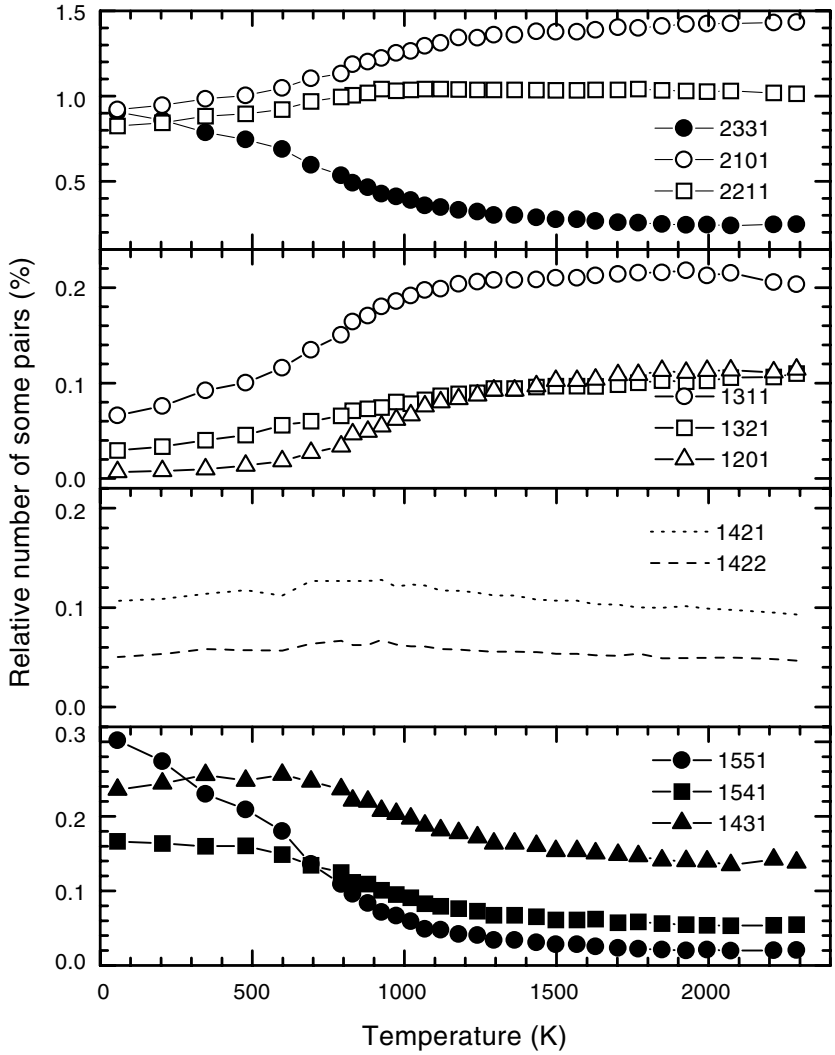

Figure 2. Relative number of main pairs as a function of temperature.

pairs (normalized by the type I pairs) as a function of temperature. From figure 2, the results concerning those pairs contributing to the first peak indicate that the first-peak sharpening originates mainly from the following feature: with lowering temperature, a large increase occurs in the number of 1551, 1541, and 1431 pairs; a large decrease occurs in the number of 1311, 1321, and 1201 pairs; however, the number of 1421 and 1422 pairs remains nearly constant. On the whole, those pairs pertaining to the relatively close-packed structure increase in number during the cooling run. These results are in good agreement with those obtained in the structural changes accompanying densification of random hard-sphere packings [4] and in the Lennard-Jones liquid and glass [2].

Three types of pair, namely 2331, 2211, and 2101 pairs, are mainly responsible for the second peak of the $g(r)$. The numbers of these pairs as a function of temperature are presented in figure 2. The 2331 pairs noticeably increase in number, whereas both 2211 and

2101 pairs decrease in number with temperature lowering. The 1551 pair, corresponding to two neighbouring atoms with five common neighbours that form a pentagon of near-neighbour contacts, can be regarded as five tetrahedra organized around a common neighbouring pair. Similarly, the 1541 pair and the 1431 pair can be regarded as five and four tetrahedra with some distortion. The 2331 pair, corresponding to two atoms (not nearest neighbours) that have three common neighbours forming a triangle of near-neighbour contacts, can be regarded as a pair of tetrahedra sharing a face. Each 1551 pair contains five 2331 pairs. Both the 1541 and the 1431 pair contain four to two tetrahedra. Note that both 1551 and 2331 pairs are characteristic of icosahedral ordering. In addition, the deviation of the 1541 pair from the 1551 pair is small; in other words, it can be regarded as a deformed fivefold structure. So the great increase in number of the 2331 pairs is consistent with the increase in number of 1551, 1541, and 1431 pairs. The 1311 and 1201 pairs contain the 2211 pairs; thus the decrease in number of the 1311 and 1201 pairs is in agreement with the decrease in number of the 2211 pairs. Therefore, the microstructural analysis allows us to infer that, as a result of the amorphization process, the content of icosahedral order and the number of tetrahedra are enhanced through the increase in the abundance of 1551, 1541, 1431, and 2331 pairs.

In order to explore the splitting mechanism of the second peak, we have calculated—in the usual way—the distribution function for those pairs contributing mainly to the second peak and plotted them in figure 3. In figure 3 three peaks, arising from the 2331, 2211, and 2101 pairs, and their sum, are denoted by P_1, P_2, P_3, and P_S respectively. A comparison between figures 3(a)–(c) indicates that:

(1) In the liquid phase, all three pairs exhibit a very broad distribution, which causes the three peaks to overlap significantly, even though they are obviously separate, so only one peak appears on the total radial distribution function.
(2) In the inherent structure of the liquid state, owing to the suppression of the vibrational motion effect, P_1, P_2, and P_3 all become narrower; P_1 and P_2 overlap totally, and they are completely separate from P_3; P_3 becomes narrower and higher. So we observe two subpeaks: the first one arises from 2331 and 2211 pairs (mainly from 2211 ones), the second one from 2101 pairs.
(3) In the amorphous state, both P_1 and P_3 become narrower and higher; P_1 is far from P_3; P_2 is located between P_1 and P_3 but it is lower in height than P_1 and P_3. Hence the 2331 pairs give the main contribution to the first subpeak while the second subpeak results from 2101 pairs. Therefore, the splitting of the second peak is mainly controlled by the width and height of these three peaks, P_1, P_2, and P_3.

In figures 4(a) and (b), we present the width[2] (a) and height (b) of these three peaks as a function of temperature (note that the closed symbols stand for the inherent structure). From the conventional structural configurations, we see that with decreasing temperature all three peaks increase in height and decrease in width, P_1 having the largest increase in height and P_3 the largest decrease in width. Interestingly, from the inherent structural configurations, both P_2 and P_3 keep a constant height and P_1 exhibits a marked increase in height with temperature lowering; both P_1 and P_3 keep an almost constant width and P_2 shows a slow decrease in width with temperature lowering. So the splitting of the second peak results from the increase of P_1 in height and the decrease of P_2 in width, but the former is predominant, i.e., the main factor is the increase in number and aggregation of the tetrahedra and the increase in number of the icosahedral order clusters.

[2] The width of the peak is measured between the points (below and above the peak centre) at which the curve has half of its maximum height. But for P_3 the width of the peak is measured between this point below and above the peak centre.

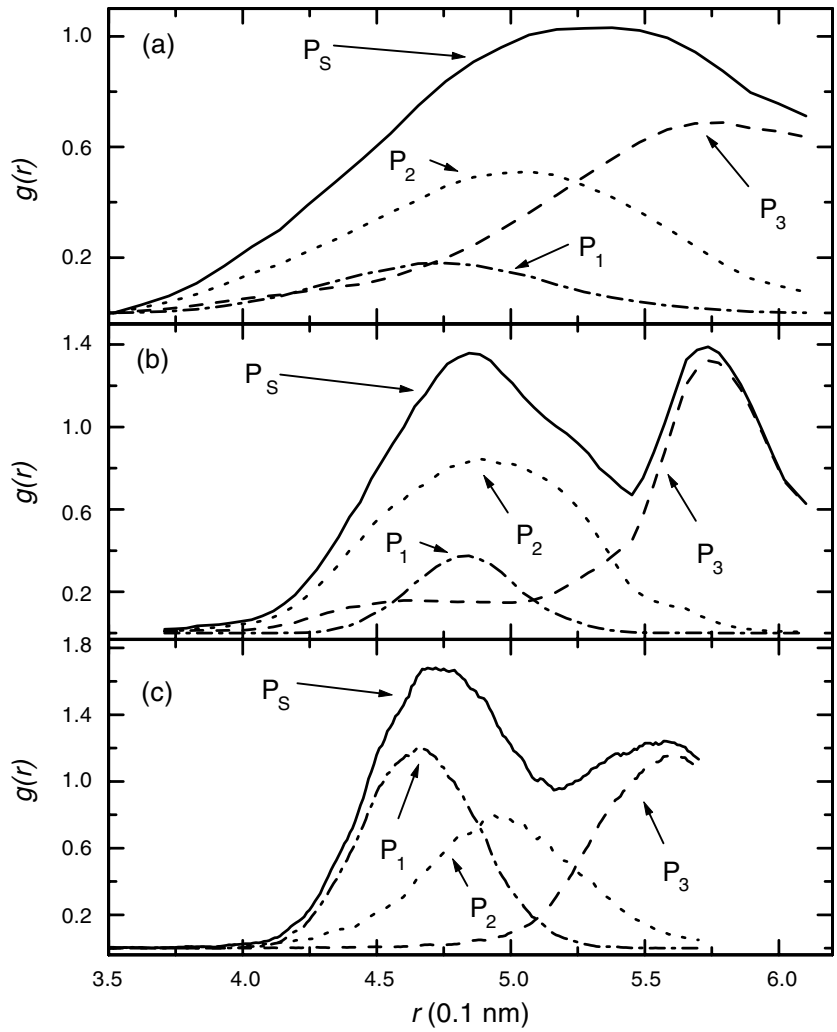

Figure 3. The main components of the second peak of the radial distribution function for liquid Al (a) and the corresponding inherent structure (b) and glass Al (c).

Various structural models, such as the microcrystalline model and the topological disorder model, have been proposed to reproduce and clarify the splitting mechanism of the second peak in $g(r)$ for both the experimental and simulated amorphous metals [1]. Despite the relatively sharp first peak and the splitting second peak observed experimentally in the $S(Q)$ or $g(r)$ of the amorphous metals, the microcrystalline model is not tenable [13]. The fundamental configuration of atoms in the amorphous state should be considered as liquid-like due to the similarity in the $g(r)$, which is supported by the previous results [1–4, 8] and our microstructural analysis of the first and second peak (through the inherent mechanism) shown in figures 1–4; for example, the sharp first peak and the splitting of the second peak appear both in the amorphous state and in the inherent structure of the liquid state. In the topological disorder model based on the dense random packing of hard spheres, amorphous structures are often described as resulting from the competition between packing of tetrahedra which maximizes

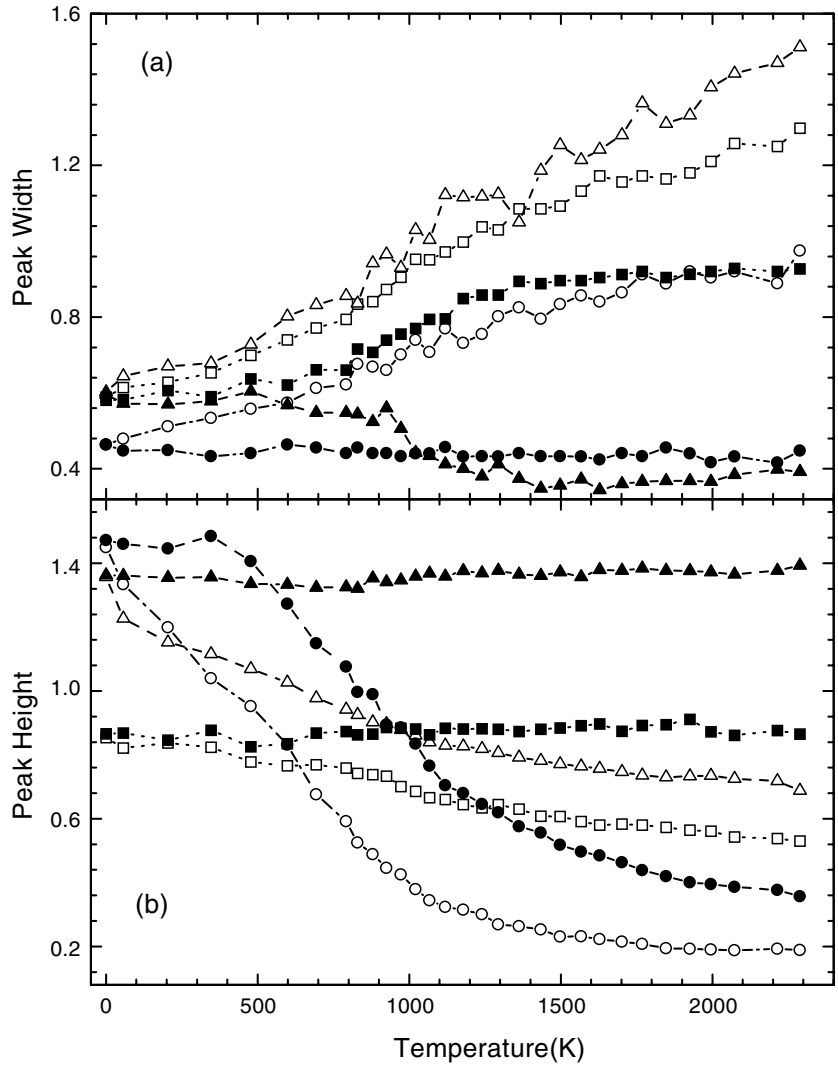

Figure 4. The width (a) and the height (b) of three peaks (P_1, P_2, and P_3—see figure 3—are denoted by circles, squares, and triangles, respectively) versus the temperature. Here open and solid symbols are used to denote the conventional and inherent structural configurations respectively.

local packing density and the frustration imposed by topological and geometrical rules to attain global space filling. The space cannot be filled by regular tetrahedra alone, though the tetrahedral arrangement of atoms achieves the densest local packing. Ichikawa [14] extended the topological disorder model that suggests the formation of distorted tetrahedra as the fundamental units of a close-packed disordered atomic distribution. The distribution of tetrahedra in the amorphous state is relatively distinct from that of liquids, the packing being more rigid in the amorphous state than in the liquid one. This is strongly supported by our present results: (1) the pairs, which pertain to the relatively close-packed structure, increase in number with decreasing temperature; and (2) as a result of amorphization, tetrahedra are enhanced in number through the increase in the abundance of 1551, 1541, 1431, and

2331 pairs. In addition, in order to explain the experimentally observed large undercoolings of pure metals, Frank first noted that a Lennard-Jones particle and its nearest neighbours prefer to form an icosahedron that consists of 20 slightly distorted tetrahedra; this icosahedral arrangement has a significantly higher binding energy than the 13-atom cluster which forms the fcc or hcp structures [15]. This argument is confirmed by several MD computational simulations [2, 16, 17], and the analysis of the experimentally determined $S(Q)$ of liquid Al–Pd–Mn alloys [18]. These works show a growing degree of icosahedral order with increasing undercooling (or decreasing temperature) of the liquid. Our present result, i.e., the increase in number of 1551 and 2331 pairs with lowering temperature, is in good agreement with Frank's argument. Very recently, using the combination of electromagnetic levitation with neutron scattering, Schenk *et al* [19] have measured the $S(Q)$ of deeply undercooled pure metallic melts (Ni, Fe, and Zr) at several temperatures. A shoulder on the right-hand side of the second oscillation is observed for all measured $S(Q)$, and this feature becomes more pronounced as temperature is lowered. From the radial distribution analysis and the simulation of the measured structure factor, the authors inferred that the icosahedral short-range order is already present above the melting point and becomes more pronounced in the undercooled state with decreasing temperature.

Therefore, our present results support and unify the topological disorder model [14] and the argument of Frank [15], and also provide the positive evidence of the experimental explanation of Schenk *et al* [19]: as the temperature lowers, the 1551, 1541, 1431, and 2331 pairs increase in number while 1311, 1321, and 1201 pairs decrease in number, which indicates that with decreasing temperature not only do the tetrahedra increase in number significantly, but also more and more tetrahedra aggregate together to form icosahedral short-range order; the marked increase in number of 1551 pairs also suggests that the distortion of tetrahedra decreases with tetrahedra aggregation. In addition, the existence of a shoulder or the splitting in the second peak of $S(Q)$ or $g(r)$ in the amorphous state, and even in the undercooled liquid state, is controlled by two factors: (i) the increase in the peak height of P_1 and (ii) the decrease in peak width of P_2, (i) being the main factor. Specifically, the main factor is the increase in number and aggregation of the tetrahedra, which in turn give rise to the presence of entities with local icosahedral order.

4. Conclusions

In summary, the microstructural analysis of the second peak of the $g(r)$ and the evolution of the pairs with temperature show that a second-peak splitting feature appears not only in the amorphous metals but also in the inherent structure of liquid metals; the first subpeak in the inherent structure of the liquid arises from 2211 and 2331 pairs, while in the amorphous state the 2331 pair is mainly responsible for this first subpeak; in both cases the second subpeak is due to the 2101 pair. With decreasing temperature the clusters with local tetrahedral and icosahedral short-range order increase in number and aggregate together, which in turn results in the presence of a shoulder on the right-hand side of the second peak or the splitting of the second peak.

Acknowledgment

This work was supported by the National Natural Sciences Foundation of China (grant No 10174082 and 10244008).

References

[1] Waseda Y 1980 *The Structure of Non-Crystalline Materials* (New York: McGraw-Hill)
[2] Jónsson H and Andersen H C 1988 *Phys. Rev. Lett.* **60** 2295
[3] Liu R S, Qi D W and Wang S 1991 *Phys. Rev.* B **45** 451
Liu R S, Liu H R, Zheng C X, Lu X Y, Peng P and Li J Y 2001 *Chin. Phys. Lett.* **18** 1383
[4] Clarke A S and Jónsson H 1993 *Phys. Rev.* E **47** 3975
[5] Posada-Amarillas A and Garzón I L 1996 *Phys. Rev.* B **53** 8363
[6] Ercolessi F and Adams J B 1994 *Europhys. Lett.* **26** 583
[7] Sun D Y and Gong X G 1998 *Phys. Rev.* B **57** 4730
[8] Liu C S, Zhu Z G, Xia J and Sun D Y 2001 *J. Phys.: Condens. Matter* **13** 1873
[9] Honeycutt J D and Andersen H C 1987 *J. Phys. Chem.* **91** 4950
[10] Stillinger F H and Weber T A 1982 *Phys. Rev.* A **25** 978
Stillinger F H and Weber T A 1983 *Phys. Rev.* A **28** 2408
[11] Stillinger F H and Weber T A 1984 *J. Chem. Phys.* **80** 4434
Weber T A and Stillinger F H 1984 *J. Chem. Phys.* **81** 5089
Weber T A and Stillinger F H 1985 *Phys. Rev.* B **31** 1954
[12] Liu C S, Zhu Z G, Xia J and Sun D Y 1999 *Phys. Rev.* B **60** 3194
Zhu Z G and Liu C S 2000 *Phys. Rev.* B **61** 9322
[13] Zallen R 1983 *The Physics of Amorphous Solids* (New York: Wiley)
[14] Ichikawa T 1975 *Phys. Status Solidi* a **29** 293
[15] Frank F C 1952 *Proc. R. Soc.* A **215** 43
[16] Steinhardt P J, Nelson D R and Ronchetti M 1983 *Phys. Rev.* B **28** 784
[17] Nóse S and Yonezawa F 1986 *J. Chem. Phys.* **84** 1803
[18] Simonet V, Hippert F, Klein H, Audier M, Bellissent R, Fischer H, Murani A P and Boursier D 1998 *Phys. Rev.* B **58** 6273
[19] Schenk T, Holland-Moritz D, Simonet V, Bellissent R and Herlach D M 2002 *Phys. Rev. Lett.* **89** 075507